universe

IMPACT FACTOR 2.6

CITESCORE 5.2

Article

Gravitational Wave Signatures of Warm Dark Matter in the Gauge Extensions of the Standard Model

Lucia A. Popa

Special Issue

Origins and Natures of Inflation, Dark Matter and Dark Energy, 2nd Edition

Edited by

Prof. Dr. Kazuharu Bamba

MDPI

https://doi.org/10.3390/universe11100343

universe

MDPI

Article

Gravitational Wave Signatures of Warm Dark Matter in the Gauge Extensions of the Standard Model

Lucia A. Popa

Institute of Space Sciences (ISS/INFLPR Subsidiary), Atomiştilor 409, RO-077125 Magurele, Ilfov, Romania; lpopa@spacescience.ro

Abstract

We studied the left-right symmetric extension of the standard model (LRSM), featuring a TeV-scale, right-handed (RH) gauge boson W_R and three RH neutrinos. This setup naturally realizes the type-II seesaw mechanism for active neutrino masses. We identified the conditions that yield sufficient entropy dilution to reconcile the keV sterile neutrino dark matter energy density with observations while inducing an early matter domination (EMD) phase. These constrained the lightest active neutrino mass to 8.59×10^{-10} eV $< m_{\nu_1} < 5.06 \times 10^{-9}$ eV. The resulting frequency-dependent suppression of the stochastic gravitational wave (GW) background was set by the mass and lifetime of the heavier RH neutrinos. Computing the signal-to-noise ratio (SNR) for future detectors, we found that a blue-tilted primordial tensor spectrum can boost the GW signal to detectable levels (SNR > 10) in experiments such as LISA, BBO, and DECIGO.

Keywords: gravitational wave background; dark matter; neutrinos; cosmological observations

1. Introduction

The gravitational wave (GW) background is one of the most significant predictions of the inflationary paradigm [1,2]. These stochastic GWs were generated by the quantum fluctuations of the metric stretched to cosmological scales during the rapid accelerated expansion of the early universe. The detailed time evolution of the Hubble rate during the expansion determines the transfer function that describes how the stochastic GWs at different frequencies were red-shifted to the present day. The resulting GW energy spectrum carries direct information about the physics of inflation and the evolution of the universe thereafter.

The shape and amplitude of the GW background are primarily determined by the primordial tensor power spectrum, which depends on two key parameters: the tensor initial amplitude A_t and the spectral index n_t [3,4]. These parameters are set by the inflationary dynamics and can vary for different inflationary scenarios. Furthermore, the spectrum is also affected by the subsequent thermal history of the universe, including the reheating phase and the radiation-dominated (RD) era [5].

In the standard slow-roll inflationary model, the GW energy spectrum is nearly scale-invariant across a wide range of frequencies. This behavior arises because the relativistic degrees of freedom remain approximately constant for modes re-entering the horizon during the RD era, resulting in minimal distortion of the spectrum. Consequently, the observation of a scale-invariant stochastic GW background would provide compelling evidence for inflation and impose constraints on both the inflationary potential and the reheating dynamics. Deviations from a scale-invariant GW spectrum can originate from two

check for updates

Academic Editor: Kazuharu Bamba

Received: 28 August 2025
Revised: 6 October 2025
Accepted: 10 October 2025
Published: 15 October 2025

Citation: Popa, L.A. Gravitational Wave Signatures of Warm Dark Matter in the Gauge Extensions of the Standard Model. *Universe* **2025**, *11*, 343. https://doi.org/10.3390/universe11100343

main sources: the tilt of the primordial tensor power spectrum [3,4,6], and modifications in the equation of the state of the early universe arising from the interaction properties of elementary particles during and after reheating [7,8].

One important effect is neutrino free-streaming, first analyzed in Ref. [9], which leads to a damping of the GW amplitude by approximately 35.5% in the frequency range 10^{-16}–10^{-10} Hz. The extension of this analysis to include all standard model (SM) particles [10] demonstrates that successive changes in the number of relativistic degrees of freedom leave distinctive imprints on the GW energy spectrum.

Moreover, a detailed thermodynamic analysis of SM particles enabled the computation of the temperature dependence of the effective degrees of freedom throughout the expansion history, where the results are provided in the form of tabulated data and fitting functions [11]. In addition, full numerical simulations of the GW spectrum across a wide frequency range, incorporating the dynamics of the inflationary scalar field, its decay during reheating, the evolution of relativistic degrees of freedom, and the anisotropic stress from photons and neutrinos, were performed in Ref. [12].

Observation of gravitational waves from black hole mergers by the LIGO and Virgo collaborations [13,14], together with the GW signals detected by pulsar timing array (PTA) experiments [15–17], has stimulated the development of various beyond standard model (BSM) scenarios for GW production. These include studies on leptogenesis [18–20], modified cosmologies and non-thermal dark matter [21–23], GW spectra arising from electroweak phase transitions [24,25], and topological defects [26]. Other works have focused on primordial black hole (PBH) formation and their associated GW signatures [27], GW generation by vector and tensor fields [28,29], and GWs produced by particle interactions in the early universe plasma [30]. Comprehensive reviews of astrophysical sources and BSM particle physics can be found in Ref. [31], while Ref. [32] discusses how current and future GW detectors may discriminate between the astrophysical and cosmological BSM signatures in the GW background.

An early matter-dominated (EMD) epoch, which can leave imprints on the GW energy spectrum, arises naturally in many BSM scenarios, in which heavy particles temporarily dominate the energy density of the universe before decaying and initiating a radiation-dominated era prior to Big Bang Nucleosynthesis (BBN).

Such a phase frequently appears in models with hidden sectors [33–36]. During the EMD phase, various mechanisms for the production of massive particles can account for the observed dark matter (DM) abundance, leading to predictions that are testable through cosmological observations and DM direct detection experiments [18,20,37].

Among the various BSM scenarios for dark matter, a sterile neutrino with a mass in the keV range and a small mixing angle with active neutrinos constitutes a well-motivated Warm Dark Matter (WDM) candidate [38–40].

Emerging from a minimal extension of the standard model, the keV-scale sterile neutrino can simultaneously explain active neutrino oscillations, the observed dark matter abundance, and the matter–antimatter asymmetry of the universe [41,42].

Several production mechanisms for keV-scale sterile neutrinos have been proposed. One of the earliest is the Dodelson–Widrow (DW) scenario [43], in which sterile neutrinos are produced via non-resonant oscillations with active neutrinos (NRPs). However, this mechanism is now ruled out by structure formation constraints, as it produces sterile neutrino velocity distributions that are too hot [44,45].

An alternative is resonant production (RP), known as the Shi–Fuller mechanism [46], in which a large lepton asymmetry enables efficient active-to-sterile neutrino conversion [47]. In this scenario, the sterile neutrino parameters required to reproduce the observed dark matter abundance are broadly consistent with current cosmological observations, including

constraints from the Local Group and high-redshift galaxy counts [47]. Nonetheless, some tension remains with Lyman-α forest data [48].

Additionally, keV sterile neutrino dark matter production via particle decays has been extensively discussed (see Ref. [49] and the references therein).

The lower mass limit of sterile neutrino dark matter is constrained by the universal Tremaine–Gunn bound [50], which applies when all dark matter is composed of sterile neutrinos. A more stringent constraint arises from analyses of the dark matter phase–space distribution in dwarf spheroidal galaxies, leading to $m_{N_1} > 1.8$ keV for sterile neutrino non-resonant production (NRP) [51]. This bound was revisited in Ref. [52] in the frame of ΛCold+Warm Dark Matter (ΛCWDM) model, where WDM in the form of sterile neutrinos represents a fraction, f_{DM}, from the total DM.

From the combined analysis of WMAP5 and Lyman$-\alpha$ datasets, it was found that if $f_{DM} = 1$ (pure ΛWDM model), then the lower bound of sterile neutrino mass in the NRP case is $M_{N_1} > 1.6$ keV (at 95%CL), which scales as $f_{DM}^{1/3}$ [53]. The same analysis shows that, below a certain threshold, f_{DM} approach has a constant value because the contribution of WDM component become too small to be constrained by the data.

A combined analysis of the CMB anisotropy and lensing data, cosmic shear observations, and low-redshift BAO measurements [54] yields a sterile neutrino mass $M_{N_1} = 7.88 \pm 0.73$ keV (68%CL) and $f_{DM} = 0.86 \pm 0.07$ (68% CL), which is consistent with the Lyman-α forest constraints that exclude $f_{\rm DM} = 1$ at 3σ [53]. A review of sterile neutrinos as a potential dark matter candidate can be found in Refs. [55,56].

Sterile neutrino dark matter is unstable. To serve as a viable dark matter candidate, its lifetime τ_{N_1} must exceed the age of the universe, $\tau_u \sim 10^{17}$ s.

A more stringent constraint on τ_{N_1} arises from its radiative decay channel $N_1 \to \nu\gamma$, in which a DM sterile neutrino decays into an active neutrino and a photon of energy $E_\gamma = M_{N_1}/2$. This photon lies within the sensitivity range of current and upcoming X-ray observatories [57–61]. The decay width of this process imposes an upper bound on the active–sterile neutrino mixing angle $\theta_1^2 \leq 1.8 \times 10^{-5} (1\,\text{keV}/M_{N_1})^5$, leading to the DM sterile neutrino lifetime $\tau_{N_1} \sim 10^{24}$ s, which is six times longer than the age of the universe [39,41].

For $M_{N_1} \geq 2$ keV, the resulting contribution of the DM sterile neutrino N_1 to the active neutrino masses, $\delta m_\nu \sim \theta_1^2 M_{N_1}$, remains below the uncertainty in the solar neutrino mass-squared difference, as indicated by the global fits to neutrino oscillation data [62]. Consequently, two additional right-handed (RH) neutrinos, N_2 and N_3, are required to reproduce the observed neutrino oscillation pattern.

In this paper, we assume an inflationary reheating scenario consistent with the normal ordering (NO) of right-handed (RH) neutrino masses $M_{N_1} < M_{N_2} < M_{N_3}$. We further assume that DM sterile neutrino N_1 is thermally produced as a relativistic particle via freeze-out, while N_2 and N_3 decouple while relativistic and then decay out of equilibrium after the freeze-out of N_1.

This scenario can be realized within the left-right symmetric extension of the standard model (LRSM), which introduces a right-handed charged gauge boson W_R with a mass at the TeV scale, as well as employs the type-II seesaw mechanism to generate active neutrino masses [63–65]. In this model, the mass spectrum of the RH neutrinos leads to the same hierarchical active neutrino spectrum. The presence of the W_R boson plays a key role in accurately predicting the dark matter relic abundance, ensuring that, for RH neutrinos that decouple while relativistic, their freeze-out temperatures, and consequently their yields, are expected to coincide to a very good approximation [66].

Once the heavier RH neutrinos become non-relativistic, they behave as matter and, if they are sufficiently long-lived, can dominate the energy density of the universe. This

results in an epoch of early matter domination (EMD), which ends with their decays and the associated release of a substantial amount of entropy.

We show that this entropy injection simultaneously dilutes the abundance of the DM sterile neutrino N_1, bringing it into agreement with observational constraints [39,66], and it also suppresses the GW energy density spectrum at scales that re-enter the horizon prior to, or during the decay of, the heavier RH neutrinos, leaving measurable imprints on the spectral shape of the gravitational wave background [18,20,37].

This paper is organized as follows. Section 2 presents the constraints and requirements for DM sterile neutrino production. Section 3 analyses the propagation of inflationary tensor perturbations as gravitational waves. Section 4 discusses the imprints left on the gravitational wave background spectrum by RH neutrino decay and evaluates the capability of various GW experiments in searching these specific signatures in terms of signal-to-noise ratio. Our conclusions are summarized in Section 5.

2. Constraints and Requirements for DM Sterile Neutrino Production

2.1. DM Sterile Neutrino Abundance

Inclusion of the RH-charged gauge boson W_R with TeV mass introduces new annihilation channels and modifies the freeze-out dynamics of RH neutrinos. The scattering of RH neutrinos with the light SM fermions, mediated by the heavy gauge bosons, keeps them in thermal equilibrium. Their freeze-out (decoupling) temperature T_f can be estimated from the out-of-equilibrium condition $\Gamma_N = H(T_f)$, where Γ_N is the interaction rate of and $H(T_f)$ is the Hubble expansion rate in the radiation-dominated universe [56,66,67]:

$$\Gamma_N(T_f) \simeq G_F^2 T_f^5 \left(\frac{M_W}{M_{W_R}}\right)^4, \qquad H(T_f) = \sqrt{\frac{4\pi g_{*f}}{45}} \frac{T_f^2}{M_{pl}}, \tag{1}$$

where g_{*f} counts the number of relativistic degrees of freedom at T_f $G_F = 1.66 \times 10^{-5}$ GeV^{-2} is the Fermi constant, $M_W = 80.34$ GeV is the mass of the W boson [68] and $M_{pl} = 1.2 \times 10^{19}$ GeV is the Planck mass. The out-of-equilibrium condition leads to [67]:

$$T_f \simeq 4\,\mathrm{MeV} \left(\frac{g_{*f}}{10.75}\right)^{1/6} \left(\frac{M_{WR}}{M_W}\right)^{4/3}. \tag{2}$$

For RH neutrinos, which freeze out while relativistic, the number density per entropy density (the yield) at T_f is as follows:

$$Y(T_f) = \frac{n_{N_1}(T_f)}{s(T_f)} \simeq \frac{1}{g_{*f}} \frac{123\zeta(3)}{4\pi^4}. \tag{3}$$

If the gauge interactions of RH neutrinos are universal, their freeze-out temperatures, and consequently their yields, are expected to coincide.

The contribution of the keV sterile neutrino N_1 with present-day energy density Ω_s to the present-day total dark matter energy density Ω_{DM} is observationally constrained to the energy density fraction $f_{DM} \leq 1$. Accordingly, using Equation (3) and taking into account that the yields of RH neutrinos are thermally conserved quantities, then f_{DM} can be written as follows:

$$f_{DM} = \frac{\Omega_s}{\Omega_{DM}} = \frac{Y_{N_1} s_0}{\Omega_{DM} \rho_c} \left(\frac{M_{N_1}}{1\,\mathrm{keV}}\right) \frac{1}{\Delta_S}, \tag{4}$$

where M_{N_1} is the sterile neutrino mass, $s_0 = 2889.2\ \mathrm{cm}^{-3}$ is the present entropy density, and $\rho_c = 1.05368 \times 10^{-5}\ \mathrm{h}^2\ \mathrm{GeV\ cm}^{-3}$ is the critical energy density. Additionally, Ω_{DM} is constrained by the cosmological observations to $\Omega_{DM} = 0.228 \pm 0.005$ at $3\,\sigma$ [69].

In the following, we adopt the sterile neutrino masses M_{N_1} in the range $1.6 \div 8$ keV, which is consistent with the observational mass bounds of the keV sterile neutrino [56].

The dilution factor Δ_s in Equation (4) accounts for the post freeze-out entropy injection needed to satisfy the observational constraint $f_{DM} \leq 1$. The value of Δ_s is required to avoid the over closure of the universe, which is given by the following:

$$\Delta_s = \frac{Y_{N_1} s_0}{\Omega_{DM} \rho_c} \left(\frac{M_{N_1}}{1\,\mathrm{keV}} \right). \tag{5}$$

2.2. Early Matter Domination (EMD) Onset and the Entropy Dilution

The large entropy injection required to achieve the correct abundance of the sterile neutrino N_1 can be generated through the decay of a heavy, long-lived particle with a relatively short lifetime [70,71]. In the LRSM, the only particles capable of such late decays with a significant impact on entropy production are the RH neutrinos N_2 and N_3.

For simplicity, in what follows, we will focus on N_2 as the diluter. In this scenario, the RH neutrino N_2 reaches thermal equilibrium at early times through its interactions with the thermal bath. After becoming non-relativistic, it behaves as a matter component and, if sufficiently long-lived, can come to dominate the energy density of the universe.

This leads to a period of early matter domination (EMD), which ends once N_2 decays, restoring a radiation-dominated (RD) universe and setting the conditions for Big Bang Nucleosynthesis (BBN).

The important stages of the thermal history in this scenario and their requirements are as follows:

- In order to achieve enough dilution, the N_2 neutrino freeze-out temperature T_f should exceed its mass; otherwise, the yield in Equation (3) receives a suppression factor $e^{-M_{N_2}/T_f}$:

$$T_f > M_{N_2}\,. \tag{6}$$

  As RH neutrino N_2 freeze out at temperature T_f is given by Equation (2), Constraint (6) leads to the bound on the RH gauge boson mass M_{WR}:

$$M_{WR} \geq 7\,\mathrm{TeV} \frac{1}{g_{*f}^{1/8}} \left(\frac{M_{N_2}}{1\,\mathrm{GeV}} \right)^{3/4}. \tag{7}$$

- The transition of N_2 to the non-relativistic regime is around at temperature $T = M_{N_2}$. At this stage, the N_2 energy density redshifts more slowly than that of radiation, scaling as $\rho_{N_2} \propto a^{-3}$ compared to $\rho_r \propto a^{-4}$, and N_2 can come to dominate the total energy density of the universe. We denote the temperature at which this transition occurs by T_{dom}, and the corresponding Hubble expansion rate by H_{dom}. The necessary condition for N_2 dominance is as follows:

$$\Gamma_{N_2} < H_{dom}\,. \tag{8}$$

  Condition $\rho_{N_2} \simeq \rho_r$ can be used to calculate H_{dom} and T_{dom} [37]:

$$H_{dom} = \frac{g_{*dom}^{2/3}}{g_N^{8/3}} H(T = M_{N_2})\,, \qquad T_{dom} = \frac{7}{4} \frac{M_{N_2}}{g_*(T_{dec})} \simeq 2\% M_{N_2}\,. \tag{9}$$

Here, g_{*dom} and $g_*(T_{dec})$ are the number of relativistic degrees of freedom at T_{dom} and T_{dec}, while $g_{*N} = 2$ accounts for the two degrees of freedom associated with the N_2 neutrino.

- Before decaying, N_2 becomes non-relativistic as long as its total decay width is smaller than the Hubble rate at temperatures around M_{N_2}, i.e., $\Gamma_{N_2} \ll H(M_{N_2})$. Assuming that the decay is instantaneous and the decay products thermalize quickly with the radiation bath, the decay temperature T_{dec} can be estimated from the condition $\Gamma_{N_2} = H(T_{dec})$ as follows:

$$T_{dec} \simeq \left(\frac{90}{8\pi^3 g_*(T_{dec})}\right)^{1/4} \sqrt{\Gamma_{N_2} M_{pl}}. \tag{10}$$

- The EMD era ends once N_2 decays and must be completed before the onset of the BBN. This constraint imposes a lower bound on the decay temperature, typically $T_{dec} > T_{BBN} = 4\,\text{MeV}$, corresponding to the following:

$$\Gamma_{N_2} > H_{BBN} \sim 10\, s^{-1}\,, \tag{11}$$

leading to the N_2 lifetime bound $\tau_{N_2} = \Gamma_{N_2}^{-1} \sim 1\, s$.

- After N_2 decay is completed, EMD ends and the universe is reheated. The entropy injection associated with the decay products dilutes the pre-existing relics. This dilution is quantified by the entropy dilution factor Δ_s, which is defined as the ratio entropy density before and after N_2 decay [18,20,37]:

$$\Delta_s \equiv \frac{s_{after}}{s_{before}}\,, \tag{12}$$

where s_{before} is the entropy density of the radiation existing from prior stages at $H = \Gamma_{N_2}$, while s_{after} is the entropy density generated by N_2 decay.
Using the energy density conservation, we have the following:

$$M_{N_2} Y_{N_2} s_{before} = \frac{3}{4} s_{after} T_{dec}\,, \tag{13}$$

and the dilution factor is obtained as

$$\Delta_s \simeq 1.8 g_f^{1/4} \frac{Y_{N_2} M_{N_2}}{\sqrt{\Gamma_{N_2} M_{pl}}}\,. \tag{14}$$

Is worth noting that, in this scenario, the freeze-out temperatures of the DM sterile neutrino N_1 coincides with that of N_2.
Combining Equations (5) and (14), we obtain the N_2 decay width as follows:

$$\Gamma_{N_2} \simeq 0.38 \times 10^{-6} g_f^{-1/2} \frac{M_{N_2}^2}{M_{pl}} \left(\frac{1\,\text{keV}}{M_{N_1}}\right)^2. \tag{15}$$

Equation (15) provides the proper entropy dilution if N_2 decouples while still relativistic, as indicated in (6), and if it satisfies BBN constraint (11). These constraints translate into a bound on the mass of N_2:

$$M_{N_2} > \left(\frac{M_1}{1\,\text{keV}}\right)(1.7 \div 10)\text{GeV}\,. \tag{16}$$

Figure 1 presents the temperature evolution in the $M_{N_1} - M_{N_2}$ parameter space across the different stages discussed above after imposing the conditions in Equations (6), (7), and (15). The N_1 energy density $\Omega_s h^2$ is also presented. For reference, this should be compared with the present energy density of the active neutrinos $\Omega_\nu \simeq 0.0011$.

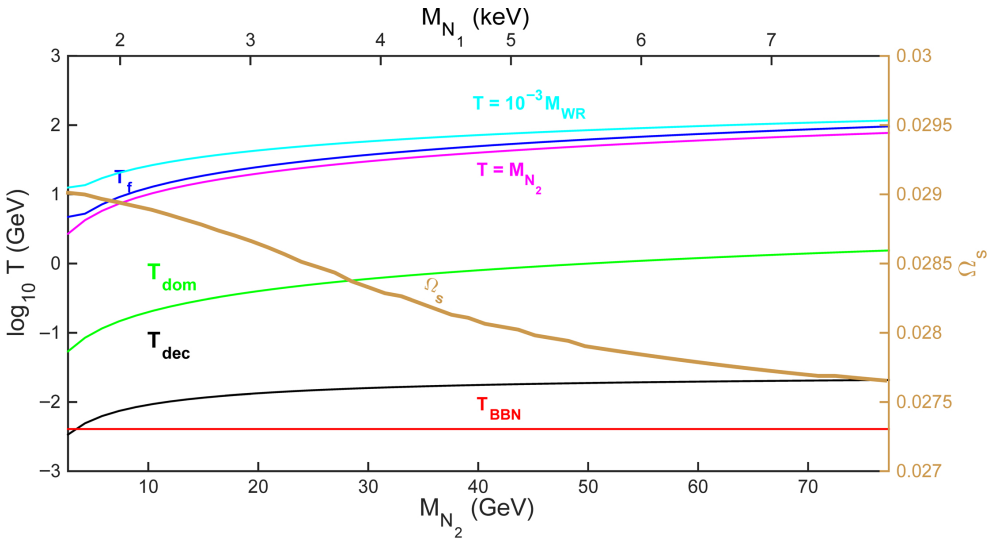

Figure 1. Temperature evolution in $M_{N_1} - M_{N_2}$ parameter space across different stages after imposing the conditions given in Equations (6), (7), and (15). The N_1 keV sterile neutrino energy density Ω_s is also presented.

In Figure 2, we show the conditions for the early matter domination (EMD) given in Equations (8) and (11).

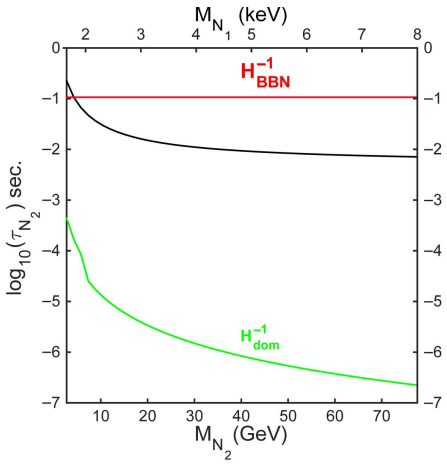

Figure 2. The conditions for the early matter domination (EMD) from Equations (8) and (11) presented in the $M_{N_1} - M_{N_2}$ parameter space. Here, $\tau_{N_2} = \Gamma_{N_2}^{-1}$ denotes the lifetime of sterile neutrino N_2, while H_{dom}^{-1} and H_{BBN}^{-1} correspond to the lifetimes of the EMD phase and of the Big Bang Nucleosynthesis (BBN), respectively.

In the left-right symmetric model (LRSM), where the active neutrino masses are generated by the type II seesaw mechanism, the mass spectrum of RH neutrinos leads to the same hierarchical spectrum for the active neutrinos, implying that the ratio of the mass eigenvalues of active and sterile neutrinos are identical [18,66]. For the normal mass ordering, this relation can be expressed as follows:

$$\frac{m_{\nu_1}}{m_{\nu_2}} = \frac{M_{N_1}}{M_{N_2}}, \qquad \frac{m_{\nu_2}}{m_{\nu_3}} = \frac{M_{N_2}}{M_{N_3}}. \tag{17}$$

The parameter space $M_{N_1} - M_{N_2}$ imposes bounds on the active neutrino mass m_{ν_1} and on the RH neutrino mass M_{N_3}. For the normal ordering, $m_{\nu_2} = \sqrt{\Delta^2 m_{sol.}} \simeq 8.6 \times 10^{-3}$ eV and $m_{\nu_3} = \sqrt{\Delta^2 m_{sol.} + \Delta^2 m_{atm}} \simeq 0.05$ eV, where $\Delta^2 m_{sol.} = 7.420^{+0.21}_{-0.20} \times 10^{-5}$ eV and $\Delta^2 m_{atm.} = 2.517^{+0.026}_{-0.028} \times 10^{-3}$ eV are the solar and atmospheric neutrino mass-squared differences obtained, respectively, from the global fit to neutrino oscillation data [62], we obtain the following:

$$8.59 \times 10^{-10}\,\text{eV} < m_{\nu_1} < 5.06 \times 10^{-9}\,\text{eV} \tag{18}$$

$$15.21\ \text{GeV} < M_{N_3} < 450.57\ \text{GeV}\,. \tag{19}$$

3. The Spectrum of the Gravitational Waves

The gravitational wave (GW) energy density spectrum today can be written as follows [20,72]:

$$\Omega_{GW}(k) = \frac{1}{12 H_0^2 a_0^2} [T^{'}(k, \tau_0)]^2 \mathcal{P}(k)\,, \tag{20}$$

where k is the GW wave number, $\tau_0 = 2/H_0$ is the conformal time today, $\mathcal{P}(k)$ is the primordial power spectrum of the tensor modes, $[T^{'}(k, \tau_0)]^2$ is the derivative of the transfer function with respect to the conformal time, $a_0 = 1$ is the present-day scale factor, and $H_0 \simeq 2.2 \times 10^{-4}\,\text{Mpc}^{-1}$ is the present Hubble expansion rate [69].

In the sub-horizon regime relevant in this paper, i.e., $k\tau_0 \gg 1$, one typically uses the approximation $[T^{'}(k, \tau_0)]^2 \sim k^2 T^2(k, \tau_0)$, leading to the following:

$$\Omega_{GW}(k) = \frac{1}{12}\left(\frac{k}{a_0 H_0}\right)^2 T^2(k) \mathcal{P}(k)\,, \tag{21}$$

The primordial power spectrum of the tensor modes $\mathcal{P}(k)$ at the pivot scale k_* can be parametrized in terms of the amplitude of the tensor modes A_T and the tensor spectral index n_T as follows:

$$\mathcal{P}(k) = A_T(k_*)\left(\frac{k}{k_*}\right)^{n_T}. \tag{22}$$

The amplitude of the tensor modes $A_T(k_*)$ is related to the amplitude of the scalar modes $A_s(k_*)$ through the following:

$$A_T(k_*) = A_s(k_*) r\,, \tag{23}$$

where r is the tensor-to-scalar ratio. In the standard slow-roll, inflation n_T satisfies the consistency relation $n_T \simeq -r/8$, leading to a red-tilted spectrum $n_T < 0$.

Alternative inflationary models and particle production models that allow departures from the consistency relation, leading to a blue-tilted spectrum ($n_T > 0$), are also discussed in the literature [73,74].

In this analysis, we adopted $r = 0.036$, as indicated by the combined PLANCK/BICEP2 observations [75], set $A_s(k_*) = 2.0989 \times 10^{-9}$ at $k_* = 0.05, \text{Mpc}^{-1}$ [69], which take n_T as the free parameter.

The transfer function $T^2(k)$ is given by the following:

$$T^2(k) = \Omega_m^2 \left(\frac{g_*(T_{hc})}{g_*^0}\right)\left(\frac{g_{*s}^0}{g_{*s}(T_{in})}\right)^{4/3}\left(\frac{3 j_1(z_k)}{z_k}\right)^2 F(k)\,, \tag{24}$$

where $g_*^0 = 3.36$ and $g_{*s}^0 = 3.91$ are the present time effective degrees of the freedom for energy density and entropy density, respectively; $\Omega_m = 0.31$ is the total matter energy

density parameter [69]; $F(k)$ is a fitting function; $j_1(z_k)$ is the spherical Bessel function; and $z_k = k\tau_0$. For $z_k \gg 1$, $j_1(z_k)$ can be approximated by $j_1(z_k) \simeq 1/(\sqrt{2}z_k)$.

The horizon crossing temperature T_{hc} associated with the scale k, can be expressed as [23]:

$$T_{hc} = \frac{k\, M_{pl}}{1.66\, a_0\, T_0\, g_*^{1/2}(T_{hc})} \left(\frac{g_{*s}(T_{hc})}{g_{*s}^0}\right)^{1/3}. \tag{25}$$

Taking $k = a_{hc}H_{hc}$ and applying the entropy conservation $g_{*s}a^3$ =const., the Hubble expansion rate at the horizon crossing H_{hc} is obtained as follows:

$$H_{hc} = \frac{k^2}{a_0^2 T_0^2} \frac{M_{pl}}{1.66} \frac{1}{g_*^{1/2}(T_{hc})} \left(\frac{g_{*s}(T_{hc})}{g_{*s}^0}\right)^{2/3}. \tag{26}$$

We use "0" and "hc" to denote quantities at the present time and at the horizon crossing, respectively, and $T_0 \simeq 2.725$ K the present cosmic microwave temperature.

The frequency f corresponding to the mode k crossing the horizon at T_{hc} is given by:

$$f = \frac{k}{2\pi a_0} = \frac{H_{hc}}{2\pi}\frac{a_{hc}}{a_0} \simeq 2.65 \times 10^{-8} \left(\frac{g_*(T_{hc})}{106.75}\right)^{1/2} \left(\frac{g_{*s}(T_{hc})}{106.75}\right)^{-1/3} \left(\frac{T_{hc}}{1\text{GeV}}\right) \text{Hz}\,. \tag{27}$$

In the standard cosmological model, the fitting function $F(k)$ from Equation (24) is given by the following [3,23,74]:

$$F_{st}(k) = T_1^2\left(\frac{k}{k_{eq}}\right) T_2^2\left(\frac{k}{k_{RH}}\right), \tag{28}$$

where the wave numbers corresponding to the matter–radiation equality and the completion of reheating are, respectively, as follows:

$$k_{eq} = 7.1 \times 10^{-2}\text{Mpc}^{-1}\Omega_m h^2\,, \tag{29}$$

$$k_{RH} = 1.7 \times 10^{14}\text{Mpc}^{-1} \left(\frac{g_{*s}(T_{RH})}{g_{*s}^0}\right)^{1/6} \left(\frac{T_{RH}}{10^7\text{GeV}}\right). \tag{30}$$

For $T_1^2(x)$, $T_2^2(x)$, we use following fitting functions [23,76]:

$$T_1^2(x) = 1 + 1.57x + 3.42x^2\,, \quad T_2^2(x) = (1 - 0.22x^{3/2} + 0.65x^2)^{-1}\,.$$

For the case with an early matter domination (EMD) phase, $F(k)$ takes the following form:

$$F_{EMD}(k) = T_1^2\left(\frac{k}{k_{eq}}\right) T_2^2\left(\frac{k}{k_{dec}}\right) T_3^2\left(\frac{k}{k_{dec}^S}\right) T_2^2\left(\frac{k}{k_{RH}^S}\right), \tag{31}$$

where

$$k_{dec} = 1.7 \times 10^{14}\text{Mpc}^{-1} \left(\frac{g_{*s}(T_{dec})}{g_{*s}^0}\right)^{1/6} \left(\frac{T_{dec}}{10^7\text{GeV}}\right) \tag{32}$$

$$k_{dec}^S = k_{dec}\Delta_s^{2/3}\,, \quad k_{RH}^S = k_{RH}\Delta_s^{-1/3}\,, \tag{33}$$

where T_{dec} denotes the N_2 sterile neutrino decay temperature given in Equation (10), T_{RH} represents the reheating temperature after inflation, and Δ_s is the entropy dilution factor defined in Equation (14).

For the fitting function $T_3^2(x)$ we used the following:

$$T_3^2(x) = 1 + 0.59x + 0.65x^2 \,. \tag{34}$$

Characteristic scales k^S_{dec} and k^S_{RH} encode key information about the EMD phase, specifically its onset and the end of the associated entropy dilution.

4. Results

4.1. DM Signatures in the Gravitational Wave Background

We computed the energy density spectrum of the gravitational waves (GWs) for the standard model and for models with an early matter domination phase (EDM).

Figures 3 and 4 present the GW energy density spectra obtained for tensor spectral index $n_T = 0$ and $n_T = 0.5$, respectively.

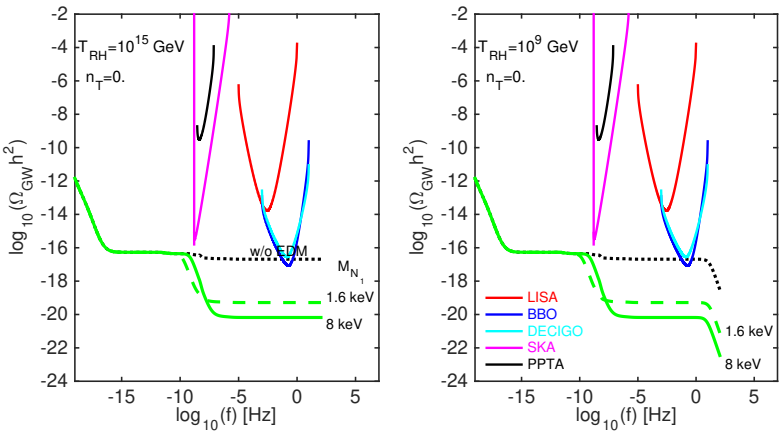

Figure 3. The gravitational wave (GW) energy density spectrum for $n_T = 0$. The (**left**) plot corresponds to $T_{RH} = 10^{15}$ GeV, while the (**right**) plot presents the results for $T_{RH} = 10^9$ GeV. In both plots, the GW spectra obtained within the standard model are shown as black dotted lines. The spectra corresponding to scenarios with an early matter domination (EMD) phase are also presented for the parameter sets $\{M_{N1}(keV), M_{N_2}(GeV), T_{dec}(GeV), \tau_{N_2}(sec.)\}$: $\{1.6, 2.7, 5.72 \times 10^{-3}, 0.224\}$ as green dashed lines, and $\{8, 80, 3.16 \times 10^{-2}, 7.07 \times 10^{-3}\}$ as green continuous lines. For comparison, the power–law-integrated sensitivity curves (PLISCs) for the future GW experiments [77,78] such as SKA, PPTA, LISA, DECIGO, and BBO, are also shown.

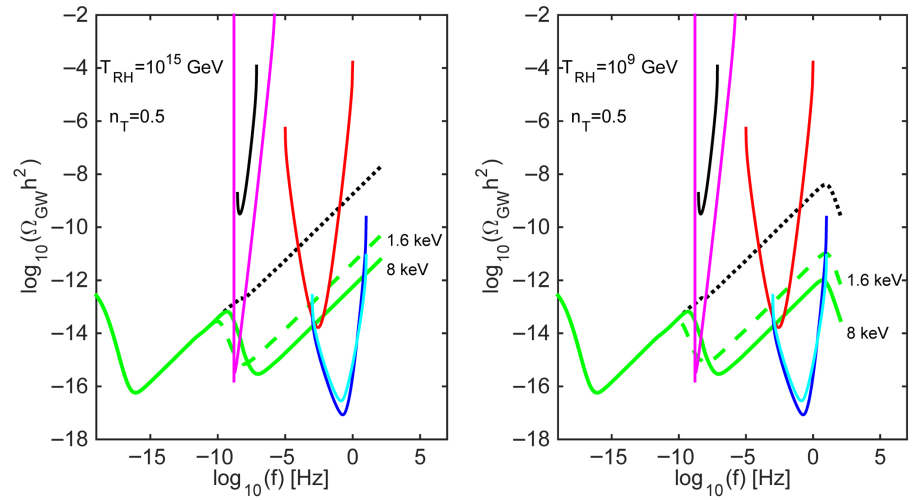

Figure 4. As in the Figure 3 for $n_T = 0.5$.

Both figures present the spectra for two benchmark reheating temperatures $T_{RH} = 10^{15}$ GeV and $T_{RH} = 10^9$ GeV. Each figure shows a characteristic suppression in

the GW spectrum that arises when entropy dilution from N_2 decay dominates, as characterized by the k^S_{dec} given in Equation (33). The suppression ends once the N_2 decay is completed at T_{dec} and occurs at k_{dec}, as defined in Equation (33). This suppression is a direct consequence of the duration of the EMD phase, which is determined by the N_2 neutrino mass M_{N_2} and is lifetime τ_N.

A larger τ_N delays the N_2 decay, lowering T_{dec} and extending the EMD duration. These dependencies are clearly illustrated in Figures 3 and 4, where they are shown by green dashed lines.

In a similar way, increasing M_{N_2} rises T_{dec}, enhancing the entropy dilution and increasing the suppression effect. These dependencies are shown in Figures 3 and 4 by green continuous lines.

The high-frequency suppression for $T_{reh} = 10^9$ GeV arises from the inflationary reheating at the characteristic scale k_{RH} given in Equation (30).

Figure 3 clearly shows that, for $n_T = 0$, the prospect of detecting the GW spectrum by the current and upcoming missions is low. However, a blue-tilted spectrum can enhance the GW spectrum, as illustrated in Figure 4 for $n_T = 0.5$.

In the standard inflationary models, the tensor spectral index is typically red, corresponding to a negative tensor tilt ($n_T < 0$). However, a number of non-standard or modified early-universe scenarios allow for a blue tilt tensor spectral index ($n_T > 0$). Examples include super-inflation [79,80], phantom inflation [81–83], Galileon inflation [84–86], and gas string inflation [87,88], as well as the multi-field and higher-curvature correction models of inflation [89,90].

A blue tilt spectral index $n_T > 0$ can enhance the GW spectrum by increasing the effective number of the relativistic degrees of freedom N_{eff} before recombination with its deviation ΔN_{eff} from the standard value $N_{eff} = 3.046$ [68]. Thus, the GW spectrum is subject to an upper bound arising from ΔN_{eff} [91]:

$$\int_{f_{min}}^{f_{max}} \frac{\mathrm{d}f}{f} \Omega_{\mathrm{GW}}(f) h^2 \leq 5.6 \times 10^{-6} \Delta N_{eff}\,, \tag{35}$$

where f_{min} is the ultraviolet cutoff that is typically 10^{-18} Hz for CMB and 10^{-10} Hz for BBN. The ultraviolet cutoff, f_{max}, represents the size of the horizon at the end of inflation and depends on the reheating temperature T_{RH} [92]. Assuming instantaneous reheating with $T_{RH} \sim 10^{15}$ GeV, one obtains $k_{end} \sim 10^{23}$ Mpc^{-1}, leading to $f_{max} \simeq 10^8$ Hz [93].

Current cosmological observations place upper limits on ΔN_{eff}, which in turn constrain the tensor spectral index via Equations (20) and (35). Specifically, the bounds are $\Delta N_{eff} \leq 0.28$ from CMB measurements [94] and $\Delta N_{eff} \leq 0.4$ from BBN data [95].

Combining the CMB and BBN constraints yields an upper limit on the tensor spectral index $n_T \leq 0.4$ (95% CL) within the standard cosmological model when assuming the current tensor-to-scalar ratio to be $r \leq 0.035$ and $T_{RH} \simeq 10^{15}$ GeV [96].

Direct measurements from ground-based interferometers, such as LIGO and VIRGO, constrain the GW energy density to $\Omega_{GW} \leq 10^{-7}$ in the frequency range 20–85.8 Hz [97], which corresponds to an upper limit on the tensor spectral index of $n_T \leq 0.52$ [94].

The tensor spectral index upper bounds are derived under the assumption that the primordial tensor power spectrum follows a power–law behavior, as given in Equation (22), which is an approach widely adopted in the literature. However, the frequencies probed by the GW experiments correspond to modes that exited the horizon near the end of inflation. Consequently, assuming a pure power–law form across all frequencies can render the estimation of n_T unreliable [98,99].

Ref. [98] demonstrates that, at high frequencies, the primordial tensor power spectrum can exhibit a strong dependence on the running of the tensor spectral index $\alpha_T = \mathrm{d}n_T/\mathrm{d}lnk$, which parameterizes the scale dependence of the tensor tilt.

The sensitivity of upcoming CMB experiments, such as CMB-S4 [100], CMB-Bharat [101], and CMB-HD [102], are expected to significantly improve the constraints on the tensor-to-scalar ratio and ΔN_{eff}. In particular, the CMB-S4 experiment aims to reach a sensitivity of $r \sim 10^{-3}$ and $\Delta N_{eff} \leq 0.05$ that, in turn, will improve the constraints on the tensor tilt.

The left panel of Figure 5 shows the tensor spectral index sensitivity curves for the future space-based interferometer experiments LISA [103,104], BBO [105,106], and DECIGO [107], and they were derived from the corresponding power–law-integrated sensitivity curves (PLISCs) that are available online in the Zenodo repository [77,78]. These results were obtained within the framework of standard cosmology for a reheating temperature of $T_{RH} = 10^{15}$ GeV and for two values of the tensor-to-scalar ratio: the current upper limit $r \leq 0.035$ and the forecasted value $r \leq 0.001$. We also include the current and projected upper bounds on n_T from the CMB and BBN observations, as well as the tensor tilt constraint from VIRGO and LIGO.

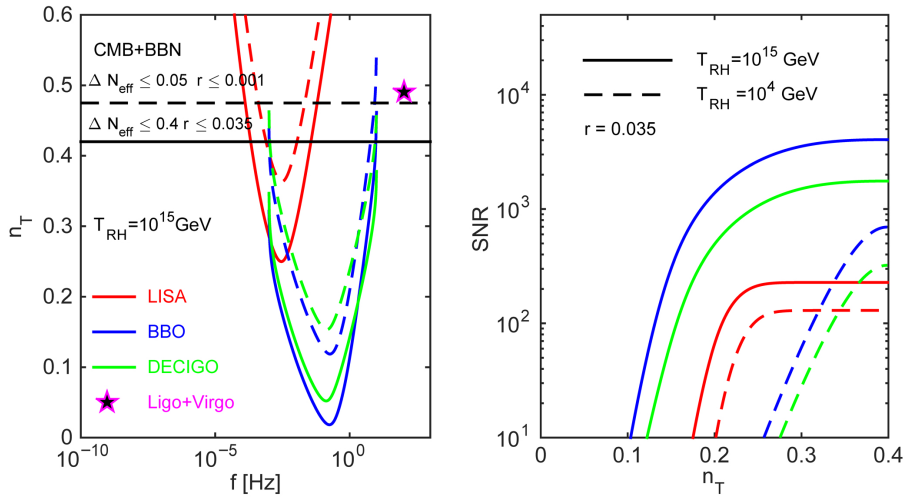

Figure 5. (**Left**): the tensor tilt (n_T) sensitivity curves for the future space-based interferometer experiments LISA, BBO, and DECIGO, which were derived from the corresponding power–law-integrated sensitivity curves (PLISCs) and are shown for $r \leq 0.035$ (solid lines) and $r \leq 0.001$ (dashed lines). Also shown are the current and projected upper bounds on n_T from the CMB and BBN observations, together with the upper limit on the n_T derived from the VIRGO and LIGO experiments. (**Right**): the allowed region in the (n_T, T_{RH}) parameter space that yields the signal-to-noise ratio SNR ≥ 10, which were obtained from the LISA, BBO, and DECIGO experiments (also see the text).

4.2. Signal-to-Noise Ratio for GW Experiments

To evaluate the capability of various GW experiments in searching for the specific early universe evolution imprints in the GW spectra described above, we computed the signal-to-noise ratio (SNR) using the PLISC files for the future space interferometers LISA, BBO, and DECIGO. The SNR is defined as follows:

$$SNR \equiv \sqrt{\tau_{obs} \int_{f_{min}}^{f_{max}} \mathrm{d}f \left(\frac{\Omega_{GW}^{EDM}(f)h^2}{\Omega_{GW}^{exp}(f)h^2} \right)^2}, \tag{36}$$

where $\Omega_{GW}^{EDM}(f)$ are the GW energy density spectra discussed in the previous section, $\Omega_{GW}^{exp}(f)$ denotes the energy density spectra derived from the PLISC signals, f_{min} and f_{max} define the operational frequency range corresponding to different experiments, and τ_{obs} is the total observation time. For a consistent sensitivity comparison, we adopted a common

observation time of $\tau_{obs} = 5$ years for all experiments and imposed the detection threshold at $SNR \geq 10$ [72].

In this analysis, we treated n_T and T_{RH} as free parameters within the region of parameter space allowed by the CMB and BBN constraints for $r \leq 0.035$, starting from $T_{RH} = 10^{15}$ GeV. The lower limit of $T_{RH} = 10^4$ GeV was imposed by the requirement that the reheating temperature must exceed the mass of the heaviest right-handed (RH) neutrino, M_{N_3}. The right panel of Figure 5 shows the allowed region (n_T, T_{RH}) that yields the signal-to-noise ratio SNR ≥ 10, which was obtained for the LISA, BBO, and DECIGO experiments. The high-frequency suppression of the $\Omega_{GW}^{EDM}(f)$ resulting from the inflationary reheating at the characteristic scale k_{RH} manifests as a decrease in the signal-to-noise ratio with decreasing T_{RH}. Since the SNR scales with T_{RH}, for clarity, the figure presents the results obtained for for $T_{RH} = 10^{15}$ GeV and $T_{RH} = 10^4$ GeV.

5. Conclusions

In this work, we considered the left-right symmetric extension of the standard model (LRSM), which introduces a right-handed charged gauge boson, W_R, with a mass at the TeV scale. This framework naturally accommodates the type-II seesaw mechanism for generating active neutrino masses.

The right-handed W_R boson plays a central role in determining the dark matter relic abundance. For RH neutrinos that decouple while still relativistic, it ensures that, to a very good approximation, their freeze-out temperatures, and thus their yields, are identical.

At later times, once the heavier RH neutrinos become non-relativistic, they behave as matter and come to dominate the energy density of the universe. This leads to a period of early matter domination (EMD), which ends when the RH neutrinos decay, releasing a significant amount of entropy.

We analyzed the conditions required to achieve the appropriate entropy dilution that both aligns the sterile neutrino dark matter abundance with observational constraints and induces an early matter domination phase. The latter leaves a characteristic, frequency-dependent suppression in the spectral shape of the stochastic gravitational wave background. Furthermore, we found that these conditions impose bounds on the lightest active neutrino mass: 8.59×10^{-10} eV $< m_{\nu_1} < 5.06 \times 10^{-9}$ eV.

We demonstrate that the frequency-dependent suppression of the gravitational wave background arises directly from the duration of the early matter domination phase, which is governed by the mass and lifetime of the heavier RH neutrino. To assess the detectability of this suppression in the GW energy spectrum by the upcoming experiments, such as SKA, LISA, BBO, and DECIGO, we evaluated the corresponding signal-to-noise ratio (SNR).

We found that a blue-tilted primordial tensor power spectrum can significantly enhance the GW energy density, enabling detection with $SNR > 10$ in experiments such as LISA, BBO, and DECIGO.

The main challenge faced in this model is the mass of right-handed gauge boson $M_{WR} \sim 10$ TeV. Theoretical considerations set a lower bound $M_{WR} > 2.5$–4 TeV [67], while direct searches, such as ATLAS and CMS, continue to raise the experimental limits on M_{W_R} [68]. Alternative approaches to avoid the overproduction of sterile neutrino dark matter within the LRSM have been proposed. For instance, Ref. [67] discusses a scenario in which all new gauge interactions are realized at the QCD scale.

Funding: This research received no external funding.

Institutional Review Board Statement: Not applicable.

Informed Consent Statement: Not applicable.

Data Availability Statement: The original contributions presented in this study are included in the article. Further inquiries can be directed to the corresponding author(s).

Acknowledgments: I would like to thank to Alexandru Dobrin for useful comments on the manuscript. The author acknowledge the use of the computing facilities at the Institute of Space Science.

Conflicts of Interest: The author declared no conflicts of interest.

References

1. Grishchuk, L.P. Amplification of gravitational waves in an isotropic universe. *Sov. J. Exp. Theor. Phys.* **1975**, *40*, 409.
2. Starobinsky, A.A. Spectrum of relic gravitational radiation and the early state of the universe. *JETP Lett.* **1979**, *30*, 682.
3. Turner, M.S.; White, M.J.; Lidsey, J.E. Tensor perturbations in infationary models as a probe of cosmology. *Phys. Rev. D* **1993**, *48*, 4613. [CrossRef] [PubMed]
4. Turner, M.S. Detectability of infation produced gravitational waves. *Phys. Rev. D* **1997**, *55*, R435. [CrossRef]
5. Smith, T.L.; Kamionkowski, M.; Cooray, A. Direct detection of the infationary gravitational wave background. *Phys. Rev. D* **2006**, *73*, 023504. [CrossRef]
6. White, M. Contribution of long-wavelength gravitational waves to the cosmic microwave background anisotropy. *Phys. Rev. D* **1992**, *46*, 4198. [CrossRef]
7. Seto, N.; Yokoyama, J. Probing the equation of state of the early universe with a space laser interferometer. *J. Phys. Soc. Jpn.* **2003**, *72*, 3082. [CrossRef]
8. Boyle, L.A.; Steinhardt, P.J. Probing the early universe with infationary gravitational waves. *Phys. Rev. D* **2008**, *77*, 063504. [CrossRef]
9. Weinberg, S. Damping of tensor modes in cosmology. *Phys. Rev. D* **2004**, *69*, 023503. [CrossRef]
10. Watanabe, Y.; Komatsu, E. Improved calculation of the primordial gravitational wave spectrum in the Standard Model. *Phys. Rev. D* **2006**, *73*, 123515. [CrossRef]
11. Ken'ichi, S.; Satoshi, S. Primordial gravitational waves, precisely: The role of thermodynamics in the Standard Model. *J. Cosmol. Astropart. Phys.* **2018**, *5*, 035. [CrossRef]
12. Kuroyanagi, S.; Chiba, T.; Sugiyama, N. Precision calculations of the gravitational wave background spectrum from infation. *Phys. Rev. D* **2009**, *79*, 103501. [CrossRef]
13. Abbott, B.P.; Abbott, R.; Abbott, T.D.; Abernathy, M.R.; Acernese, F.; Ackley, K.; Cavalieri, R. Observation of Gravitational Waves from a Binary Black Hole Merger. *Phys. Rev. Lett.* **2016**, *116*, 061102. [CrossRef] [PubMed]
14. Abbott, B.P.; Abbott, R.; Abbott, T.D.; Abernathy, M.R.; Acernese, F.; Ackley, K.; Chamberlin, S.J. GW151226: Observation of Gravitational Waves from a 22-Solar-Mass Binary Black Hole Coalescence. *Phys. Rev. Lett.* **2016**, *116*, 241103. [CrossRef]
15. Weltman, A.; Bull, P.; Camera, S.; Kelley, K.; Padmanabhan, H.; Pritchard, J.; Gaensler, B.M. Fundamental physics with the Square Kilometre Array. *Publ. Astron. Soc. Austral.* **2020**, *37*, 2. [CrossRef]
16. Lentati, L.; Taylor, S.R.; Mingarelli, C.M.; Sesana, A.; Sanidas, S.A.; Vecchio, A.; Verbiest, J.P. European Pulsar Timing Array Limits on an Isotropic Stochastic Gravitational-Wave Background. *Mon. Not. R. Astron. Soc.* **2015**, *453*, 2598. [CrossRef]
17. Agazie, G.; Anumarlapudi, A.; Archibald, A.M.; Arzoumanian, Z.; Baker, P.T.; Bécsy, B.; Young, O. The NANOGrav 15 yr Data Set: Evidence for a Gravitational-wave Background. *Astrophys. J. Lett.* **2023**, *951*, L8. [CrossRef]
18. Giudice, G.F.; Riotto, A.; Tkachev, I.; Peloso, M. Production of massive fermions at preheating and leptogenesis. *J. High Energy Phys.* **1999**, *8*, 014. [CrossRef]
19. Buchmuller, W.; Domcke, V.; Kamada, K.; Schmitz, K. The Gravitational Wave Spectrum from Cosmological B-L Breaking. *J. Cosmol. Astropart. Phys.* **2013**, *10*, 003. [CrossRef]
20. Berbig, M.; Ghoshal, A. Impact of high-scale Seesaw and Leptogenesis on inflationary tensor perturbations as detectable gravitational waves. *J. High Energy Phys.* **2023**, *5*, 172. [CrossRef]
21. Ghoshal, A.; Heurtier, L.; Paul, A. Signatures of non-thermal dark matter with kination and early matter domination. Gravitational waves versus laboratory searches. *J. High Energy Phys.* **2022**, *12*, 105. [CrossRef]
22. Bernal, N.; Ghoshal, A.; Hajkarim, F.; Lambiase, G. Primordial Gravitational Wave Signals in Modified Cosmologies. *J. Cosmol. Astropart. Phys.* **2020**, *11*, 51. [CrossRef]
23. Nakayama, K.; Saito, S.; Suwa, Y.; Yokoyama, J. Probing reheating temperature of the universe with gravitational wave background. *J. Cosmol. Astropart. Phys.* **2006**, *6*, 20. [CrossRef]
24. Eichhorn, A.; Lumma, A.; Pawlowski, J.M.; Scherer, M.M.; Reichert, F.J.T.; Yamada, K. Universal gravitational-wave signatures from heavy new physics in the electroweak sector. *SciPost Phys.* **2020**, *9*, 41. [CrossRef]
25. Dent, J.B.; Dutta, B.; Rai, M. Imprints of early universe cosmology on gravitational waves. *J. High Energy Phys.* **2025**, *3*, 98. [CrossRef]

26. Gouttenoire, Y.; Servant, E.; Simakachorn, P. BSM with cosmic strings: heavy, up to EeV mass, unstable particles. *J. Cosmol. Astropart. Phys.* **2020**, *7*, 32. [CrossRef]
27. Escriva, A.; Kuhnel, F.; Tada, Y. Primordial Black Holes Messenger of the Dark Universe. *Symmetry* **2024**, *16*, 1487. [CrossRef]
28. Tsukada, L.; Brito, R.; East, W.E.; Siemonsen, N. Modeling and searching for a stochastic gravitational-wave background from ultralight vector bosons. *Phys. Rev. D* **2021**, *103*, 083005. [CrossRef]
29. Guo, H.-K.; Jiang, J.; Huang, G.-Y. Probing ultralight tensor dark matter with the stochastic gravitational-wave background. *J. Cosmol. Astropart. Phys.* **2024**, *3*, 006.
30. Muia, F.; Quevedo, F.; Schachner, A.; Villa, M.A.G. Testing BSM Physics with Gravitational Waves. *J. Cosmol. Astropart. Phys.* **2023**, *9*, 006. [CrossRef]
31. Sakellariadou, M. Gravitational Waves: The Theorist's Swiss Knife. *Universe* **2018**, *4*, 132. [CrossRef]
32. Ellis, J. Gravitational Waves: Echoes of the Biggest Bangs Since the Big Bang and/or BSM Physics? *Universe* **2025**, *11*, 213. [CrossRef]
33. Dror, J.A.; Kuik, E.; Ng, W.H. Co-Decaying Dark Matter. *Phys. Rev. Lett.* **2016**, *117*, 211801. [CrossRef]
34. Berlin, A.; Hooper, D.; Krnjaic, G. Thermal dark matter from a highly decoupled sector. *Phys. Rev. D* **2016**, *94*, 095019. [CrossRef]
35. Dror, J.A.; Kuik, E.; Melcher, B.; Watson, S. Concentrated dark matter: Enhanced small-scale structure from co-decaying dark matter. *Phys. Rev. D* **2018**, *97*, 063524. [CrossRef]
36. Cirelli, M.; Gouttenoire, Y.; Petraki, K.; Sala, F. Homeopathic Dark Matter, or how diluted heavy substances produce high energy cosmic rays. *J. Cosmol. Astropart. Phys.* **2019**, *1902*, 014. [CrossRef]
37. Allahverdi, R.; Osiński, J.K. Early Matter Domination from Long-Lived Particles in the Visible Sector. *Phys. Rev. D* **2022**, *105*, 023502. [CrossRef]
38. Abazajian, K.N.; Fuller, G.M.; Patel, M. Sterile neutrino hot, warm and cold dark matter. *Phys. Rev. D* **2001**, *64*, 023501. [CrossRef]
39. Boyarsky, A.; Ruchayskiy, O.; Shaposhnikov, M. The Role of sterile neutrinos in cosmology and astrophysics. *Annu. Rev. Nucl. Part. Sci.* **2009**, *59*, 191–214. [CrossRef]
40. Kusenko, A. Sterile neutrinos: The Dark side of the light fermions. *Phys. Rep.* **2009**, *481*, 1–28. [CrossRef]
41. Asaka, T.; Blanchet, S.; Shaposhnikov, M. The MSW dark matter and neutrino masses. *Phys. Lett. B* **2005**, *631*, 151. [CrossRef]
42. Asaka, T.; Shaposhnikov, M. The νMSM, dark matter and baryon asymmetry of the universe. *Phys. Lett. B* **2005**, *620*, 17. [CrossRef]
43. Dodelson, S.; Widrow, L.M. Sterile-neutrinos as dark matter. *Phys. Rev. Lett.* **1994**, *72*, 17. [CrossRef]
44. Canetti, L.; Drewes, M.; Frossard, T.; Shaposhnikov, M. Dark matter, baryogenesis and neutrino oscillations from right-handed neutrinos. *Phys. Rev. D* **2013**, *87*, 093006. [CrossRef]
45. Merle, A.; Niro, V. Influence of a keV sterile neutrino on neutrinoless double beta decay: How things changed in recent years. *Phys. Rev. D* **2013**, *88*, 113004. [CrossRef]
46. Shi, X.D.; Fuller, G.M. A New dark matter candidate: Nonthermal sterile neutrinos. *Phys. Rev. Lett.* **1999**, *82*, 2832. [CrossRef]
47. Laine, M.; Shaposhnikov, M. Sterile neutrino dark matter as a consequence of MSM-induced lepton asymmetry. *J. Cosmol. Astropart. Phys.* **2008**, *6*, 031. [CrossRef]
48. Merle, A.; Schneider, A. Production of Sterile Neutrino dark matter and the 3.5 keV line. *Phys. Lett. B* **2015**, *749*, 283. [CrossRef]
49. Adhikari, R.; Agostini, M.; Ky, N.A.; Araki, T.; Archidiacono, M.; Bahr, M.; Zuber, K. A White Paper on keV sterile neutrino Dark Matter. *J. Cosmol. Astropart. Phys.* **2017**, *1*, 025. [CrossRef]
50. Tremaine, S.; Gunn, J.E. Dynamical role of light neutral leptons in cosmology. *Phys. Rev. Lett.* **1979**, *42*, 407. [CrossRef]
51. Boyarsky, A.; Ruchayskiy, O.; Iakubovskyi, D. A lower bound on the mass of dark matter particles. *J. Cosmol. Astropart. Phys.* **2009**, *3*, 005. [CrossRef]
52. Boyarsky, A.; Lesgourgues, J.; Ruchayskiy, O.; Viel, M. Lyman-α constraints on warm and on warm-plus-cold dark matter models. *J. Cosmol. Astropart. Phys.* **2009**, *0905*, 012. [CrossRef]
53. Palazzo, A.; Cumberbatch, D.; Slosar, A.; Silk, J. Sterile neutrinos as subdominant warm dark matter. *Phys. Rev. D* **2007**, *76*, 103511. [CrossRef]
54. Popa, L.A. Dark Matter Sterile Neutrino from Scalar Decays. *Universe* **2021**, *7*, 309. [CrossRef]
55. Abazajian, K.N. Sterile neutrinos in cosmology. *Phys. Rep.* **2017**, *711–712*, 1–28. [CrossRef]
56. Boyarsky, A.; Drewes, M.; Lasserre, T.; Mertens, S.; Ruchayskiy, O. Sterile neutrino Dark Matter. *Prog. Part. Nucl. Phys.* **2019**, *104*, 1–45. [CrossRef]
57. Jeltema, T.E.; Profumo, S. Discovery of a 3.5 keV line in the Galactic Centre and a critical look at the origin of the line across astronomical targets. *Mon. Not. R. Astron. Soc.* **2015**, *450*, 2143. [CrossRef]
58. Riemer-Sorensen, S. Constraints on the presence of a 3.5 keV dark matter emission line from Chandra observations of the Galactic centre. *Astron. Astrophys.* **2016**, *590*, A71. [CrossRef]
59. Loewenstein, M.; Kusenko, A.; Biermann, P.L. New Limits on Sterile Neutrinos from Suzaku Observations of the Ursa Minor Dwarf Spheroidal Galaxy. *Astrophys. J.* **2009**,*700*, 426.

60. Urban, O.; Werner, N.; Allen, S.W.; Simionescu, A.; Kaastra, J.S.; Strigari, L.E. A Suzaku Search for Dark Matter Emission Lines in the X-ray Brightest Galaxy Clusters. *Mon. Not. R. Astron. Soc.* **2015**, *451*, 2447. [CrossRef]
61. Malyshev, D.; Neronov, A.; Eckert, D. Constraints on 3.55 keV line emission from stacked observations of dwarf spheroidal galaxies. *Phys. Rev. D* **2014**, *90*, 1035062014. [CrossRef]
62. Esteban, I.; Gonzalez-Garcia, M.C.; Maltoni, M.; Schwetz, T.; Zhou, A. The fate of hints: Updated global analysis of three-flavor neutrino oscillations. *J. High Energy Phys.* **2020**, *09*, 178. [CrossRef]
63. Zhang, Y.; An, H.; Ji, X.; Mohapatra, R.N. CP Violation in Minimal Left-Right Symmetric Model and Constraints on the Right-Handed Scale. *Nucl. Phys. B* **2008**, *802*, 247. [CrossRef]
64. Maiezza, A.; Nemevsek, M.; Nesti, F.; Senjanovi, G. Left-Right Symmetry at LHC. *Phys. Rev. D* **2010**, *82*, 055022. [CrossRef]
65. Magg, M.; Wetterich, C. Neutrino Mass Problem And Gauge Hierarchy. *Phys. Lett. B* **1980**, *94*, 61. [CrossRef]
66. Bezrukov, F.; Hettmansperger, H.; Lindner, M. keV sterile neutrino Dark Matter in gauge extensions of the Standard Model. *Phys. Rev. D* **2010**, *81*, 085032. [CrossRef]
67. Nemevšek, M.; Senjanović, G.; Zhang, Y. Warm dark matter in low scale left-right theory. *J. Cosmol. Astropart. Phys.* **2012**, *07*, 006. [CrossRef]
68. Navas, S.; Amsler, C.; Gutsche, T.; Hanhart, C.; Hernandez-Rey, J.J.; Lourenco, C.; Masoni, A.; Mikhasenko, M.; Mitchell, R.E.; Patrignani, C.; et al. Particle Data Group. *Phys. Rev. D* **2024**, *110*, 030001. [CrossRef]
69. Aghanim, N. Planck 2018 results. VI. Cosmological parameters. *Astron. Astrophys.* **2020**, *641*, A6.
70. Nemevšek, M.; Zhang, Y. Dark Matter Dilution Mechanism through the Lens of Large Scale Structure. *Phys. Rev. Lett.* **2023** *130*, 121002. [CrossRef]
71. Nemevšek, M.; Zhang, Y.; Anatomy of diluted dark matter in the minimal left-right symmetric model. *Phys. Rev. D* **2024**, *109*, 056021. [CrossRef]
72. Caprini, C.; Figueroa, D.G. Cosmological backgrounds of gravitational waves. *Class. Quantum Gravity* **2018**, *35*, 163001. [CrossRef]
73. Mukohyama, S.; Namba, R.; Peloso, M.; Shiu, G. Blue Tensor Spectrum from Particle Production during Inflation. *J. Cosmol. Astropart. Phys.* **2014**, *8*, 36. [CrossRef]
74. Kuroyanagi, S.; Takahashi, T.; Yokoyama, S. Blue-tilted inflationary tensor spectrum and reheating in the light of NANOGrav results. *J. Cosmol. Astropart. Phys.* **2021**, *1*, 71. [CrossRef]
75. Ade, P.A.; Ahmed, Z.; Amiri, M.; Barkats, D.; Thakur, R.B.; Bischoff, C.A.; BICEP/Keck Collaboration. Improved Constraints on Primordial Gravitational Waves using Planck, WMAP, and BICEP/Keck Observations through the 2018 Observing Season. *Phys. Rev. Lett.* **2021**, *127*, 151301. [CrossRef]
76. Kuroyanagi, S.; Takahashi, T.; Yokoyama, S. Blue-tilted Tensor Spectrum and Thermal History of the Universe. *J. Cosmol. Astropart. Phys.* **2015**, *2*, 003. [CrossRef]
77. Schmitz, K. New Sensitivity Curves for Gravitational-Wave Experiments. *arXiv preprint* **2020**, arXiv:2002.04615.
78. Schmitz, K. New Sensitivity Curves for Gravitational-Wave Signals from Cosmological Phase Transitions. *J. High Energy Phys.* **2021**, *1*, 097. [CrossRef]
79. Basak, A.; Shankaranarayanan, S. Super-inflationary phase transitions and blue tensor spectrum. *JCAP* **2010**, *11*, 021.
80. Nojiri, S.; Odintsov, S.D.; Paul, T. Early and late universe holographic cosmology from a new generalized entropy. *Phys. Lett. B* **2022**, *831*, 137189. [CrossRef]
81. Liu, Z.G.; Zhang, J.; Piao, Y.S. Phantom inflation with a steplike potential. *Phys. Lett. B* **2011**, *697*, 407. [CrossRef]
82. Richarte, M.G.; Kremer, G.M. Cosmological perturbations in transient phantom inflation scenarios. *Eur. Phys. J. C* **2017**, *77*, 51. [CrossRef]
83. Iqbal, A.; Hussain, I.; Javed, F. Confronting phantom inflation with Planck data. *Astrophys. Space Sci.* **2018**, *363*, 222. [CrossRef]
84. Kobayashi, T.; Yamaguchi, M.; Yokoyama, J. G-inflation: Inflation driven by the Galileon field. *Phys. Rev. Lett.* **2010**, *105*, 231302. [CrossRef] [PubMed]
85. Choudhury, S.; Karde, A.; Panda, S.; Sami, M. Primordial non-Gaussianity from ultra slow-roll Galileon inflation. *J. Cosmol. Astropart. Phys.* **2024**, *01*, 012. [CrossRef]
86. Choudhury, S.; Karde, A.; Panda, S.; Sami, M. Scalar induced gravity waves from ultra slow-roll Galileon inflation. *Nucl. Phys. B* **2024**, *1007*, 116678. [CrossRef]
87. Brandenberger, R.H. String Gas Cosmology. *arXiv preprint* **2008**, arXiv:0808.0746.
88. Brandenberger, R.H. Superstring cosmology—A complementary review. *J. Cosmol. Astropart. Phys.* **2023**, *11*, 019. [CrossRef]
89. Smith, A.; Mylova, M.; Brax, P.; Bruck, C.v.; Burgess, C.P.; Davis, A.-C. CMB implications of multi-field axio-dilaton cosmology. *J. Cosmol. Astropart. Phys.* **2024**, *12*, 058. [CrossRef]
90. Geller, S.R.; McDonough, W.Q.E.; Kaiser, D.I. Primordial black holes from multifield inflation with nonminimal couplings. *Phys. Rev. D* **2024**, *106*, 063535. [CrossRef]
91. Maggiore, M. Gravitational wave experiments and early universe cosmology. *Phys. Rept.* **2000**, *331*, 283. [CrossRef]

92. Meerburg, P.D.; Hlozek, R.; Hadzhiyska, B.; Meyers, J. Multi-wavelength constraints on the inflationary consistency relation. *Phys. Rev. D* **2015**, *91*, 103505. [CrossRef]
93. Cabass, G.; Pagano, L.; Salvati, L.; Gerbino, M.; Giusarma, E.; Melchiorri, A. Updated Constraints and Forecasts on Primordial Tensor Modes. *Phys. Rev. D* **2016**, *93*, 063508. [CrossRef]
94. Akrami, Y.; Arroja, F.; Ashdown, M.; Aumont, J.; Baccigalupi, C.; Ballardini, M.; Savelainen, M. Planck 2018 results. X. Constraints on inflation. *Astron. Astrophys.* **2018**, *641*, A10.
95. Cyburt, R.H.; Fields, B.D.; Olive, K.A.; Yeh, T.-H. Big Bang Nucleosynthesis: 2015. *Rev. Mod. Phys.* **2016**, *88*, 015004. [CrossRef]
96. Giare, W.; Forconi, M.; Valentino, E.D.; Melchiorri, A. Towards a reliable calculation of relic radiation from primordial gravitational waves. *Mon. Not. R. Astron. Soc.* **2023**, *520*, 1757. [CrossRef]
97. Abbott, B.P.; Abbott, R.; Abbott, T.D.; Acernese, F.; Ackley, K.; Adams, C.; Cao, J. GW170104: Observation of a 50-Solar-Mass Binary Black Hole Coalescence at Redshift 0.2. *Phys. Rev. Lett* **2017**, *118*, 121101. [CrossRef]
98. Giare, W.; Melchiorri, A. Probing the early Universe with gravitational waves from inflation. *Phys. Lett. B* **2021**, *815*, 136137. [CrossRef]
99. Kinney W.H. Gravitational Wave Direct Detection does not Constrain the Tensor Spectral Index at CMB Scales. *Open J. Astrophys.* **2021**, *4*, 5. [CrossRef]
100. Abazajian, K.; Addison, G.E.; Adshead, P.; Ahmed, Z.; Akerib, D.; Ali, A.; Millea, M. CMB-S4: Forecasting Constraints on Primordial Gravitational Waves. *Astrophys. J.* **2022**, *926*, 54. [CrossRef]
101. Adak, D.; Sen, A.; Basak, S.; Delabrouille, J.; Ghosh, T.; Rotti, A.; Souradeep, T. B-mode forecast of CMB-Bharat. *Mon. Not. R. Astron. Soc.* **2022**, *514*, 3002. [CrossRef]
102. Aiola, S.; Akrami, Y.; Basu, K.; Boylan-Kolchin, M.; Brinckmann, T.; Bryan, S.; HD Collaboration. Snowmass2021 CMB-HD White Paper. *arXiv* **2022**, arXiv:2203.05728.
103. Amaro-Seoane, P.; Audley, H.; Babak, S.; Baker, J.; Barausse, E.; Bender, P.; Zweifel, P. Laser Interferometer Space Antenna. *arXiv* **2017**, arXiv:1702.00786. [CrossRef]
104. Baker, J.; Bellovary, J.; Bender, P.L.; Berti, E.; Caldwell, R.; Camp, J.; Ziemer, J. The Laser Interferometer Space Antenna: Unveiling the Millihertz Gravitational Wave Sky. *arXiv* **2019**, arXiv:1907.06482. [CrossRef]
105. Crowder, J.; Cornish, N.J. Beyond LISA: Exploring future gravitational wave missions. *Phys. Rev. D* **2005**, *72*, 083005. [CrossRef]
106. Corbin, V.; Cornish, N.J. Detecting the cosmic gravitational wave background with the big bang observer. *Class. Quant. Grav.* **2006**, *23*, 2435. [CrossRef]
107. Isoyama, S.; Nakano, H.; Nakamura, T. Multiband Gravitational-Wave Astronomy: Observing binary inspirals with a decihertz detector, B-DECIGO. *Prog. Theor. Exp. Phys.* **2018**, *2018*, 073E01. [CrossRef]